Lithium Storage

Deutsche Ausgabe: DOI: 10.1002/ange.201602653
Internationale Ausgabe: DOI: 10.1002/anie.201602653

Electrolytic Formation of Crystalline Silicon/Germanium Alloy Nanotubes and Hollow Particles with Enhanced Lithium-Storage Properties

Wei Xiao, Jing Zhou, Le Yu, Dihua Wang, and Xiong Wen (David) Lou**

Abstract: *Crystalline silicon(Si)/germanium(Ge) alloy nanotubes and hollow particles are synthesized for the first time through a one-pot electrolytic process. The morphology of these alloy structures can be easily tailored from nanotubes to hollow particles by varying the overpotential during the electro-reduction reaction. The continuous solid diffusion governed by the nanoscale Kirkendall effect results in the formation of inner void in the alloy particles. Benefitting from the compositional and structural advantages, these SiGe alloy nanotubes exhibit much enhanced lithium-storage performance compared with the individual solid Si and Ge nanowires as the anode material for lithium-ion batteries.*

New electrical energy storage (EES) technologies are critical to enable modern civilization to secure a sustainable, distributed energy supply for the society. Amongst them, lithium-ion batteries (LIBs) are becoming a key-enabling technology for electronic consumables and the emerging electric vehicles.[1–3] Lithium-alloying materials, such as silicon (Si) and germanium (Ge) have been considered as the forerunners to replace the state-of-the-art graphite-based anodes.[4–12] Importantly, Si anodes exhibit the highest theoretical capacity (3580 $mAh\,g^{-1}$) among various candidates. Meanwhile, Ge-based materials have faster ion diffusion (400-times faster than Si) and much better electrical conductivity (ten thousand times higher than Si).[13] Recently, it has been demonstrated that the combination of Si and Ge (Si/Ge) either by alloying Si with Ge (SiGe) or by employing Si–Ge heterostructures can take full advantages of the merits from these two materials with modified physicochemical properties and enhanced lithium-storage performance.[14–19] However, dramatic volume changes associated with the lithium insertion and extraction reactions (up to 400%) lead to pulverization of the Si/Ge based materials and thus poor cycling life of electrodes.[20]

One typical approach to overcome this problem is the design and synthesis of complex micro-/nanostructured electrodes that can maintain their structural integration after many cycles.[21] Notably, a diversity of hollow nanostructures with distinct geometric shapes, such as nanotubes or hollow spheres has been extensively investigated.[22–25] It is believed the void space in hollow architectures would efficiently alleviate the structural strain during charge/discharge cycling and prevent the aggregation of electrode materials. Constructions of hollow-structured Si, Ge, or Si/Ge materials are usually achieved through typical multistep hard-templating methods, which involve the formation of template with desired shapes, the subsequent coating process of the target materials and the removal of the inner template in different chemical environments.[5,26,27] For example, Paik and co-workers developed novel arrays of sealed Si nanotubes using arrays of dense ZnO nanorods as the sacrificial templates.[26] Cho and co-workers reported the synthesis of ordered three-dimensional (3D) porous nanoparticle assemblies prepared by etching a thermally annealed physical mixture of SiO_2 and ethyl-capped Ge gels at 800 °C.[6] Patolsky and Ben-Ishai have reported the synthesis of SiGe alloy nanotubes by employing the Ge nanowire as templates in an ultrahigh vacuum chemical vapor deposition (UHV-CVD) system.[27] The inner Ge core is selectively removed by the following wet-chemical etching process. Although quite efficient, these synthetic routes entail complicated processes, which retard large-scale deployment of hollow nanostructured Si/Ge materials. Therefore, it is of great importance and urgency to develop a direct approach for massive production of these unique hollow particles for LIBs.

Herein, we report an unprecedented strategy for the controllable synthesis of SiGe hollow nanostructures including nanotubes and hollow particles through a one-pot electro-reduction of solid mixed oxides in molten chlorides. An interesting structural evolution from nascent Ge solid particles to ultimate crystalline SiGe hollow structures through a solid diffusion process can be observed without alternation of the reaction environment. As expected, the as-obtained SiGe alloy hollow structures provide apparent superiorities over the solid Si and Ge counterparts with much enhanced capacity and excellent cycling stability when evaluated as an anode material for LIBs.

Taking the preparation of SiGe alloy nanotubes as the example, the general protocol for the one-pot electrolytic formation of SiGe hollow structures is schematically illustrated in Figure 1. According to the previous reports, direct electro-reduction of individual solid SiO_2 and GeO_2 in molten chlorides can create metallic Si and Ge with well-defined

[*] Dr. W. Xiao, J. Zhou, Prof. D. H. Wang
School of Resource and Environmental Sciences, Hubei International Scientific and Technological Cooperation Base of Sustainable Resource and Energy, Wuhan University
Wuhan 430072 (PR China)
E-mail: wangdh@whu.edu.cn
Dr. L. Yu, Prof. X. W. Lou
School of Chemical and Biomedical Engineering, Nanyang Technological University
62 Nanyang Drive, Singapore 637459 (Singapore)
E-mail: xwlou@ntu.edu.sg
Homepage: http://www.ntu.edu.sg/home/xwlou/

Supporting information for this article can be found under: http://dx.doi.org/10.1002/anie.201602653.

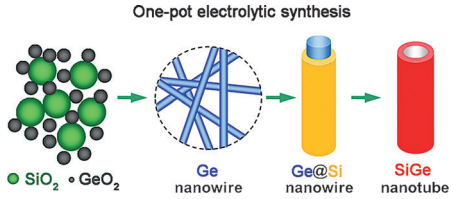

Figure 1. Schematic illustration on the synthesis of SiGe nanotubes from electro-reduction of the mixture of solid SiO_2 and GeO_2 particles in molten chlorides. This one-pot electrolytic synthesis includes the formation of Ge nanowires, Ge@Si core–shell structures, and the subsequent solid diffusion process for the formation of SiGe nanotubes.

structures.[28–34] When the mixture of SiO_2 and GeO_2 is involved, the de-oxidation of GeO_2 is thermodynamically favorable according to the change in Gibbs free energy (ΔG) and standard decomposition voltage (V^0) for the reduction process of Ge and Si at 800 °C in the Equations (1) and (2):

$$GeO_2(s) = Ge(s) + O_2(g) \quad \Delta G = 373.5\ kJ\ mol^{-1},\ V^0 = 0.97\ V \tag{1}$$

$$SiO_2(s) = Si(s) + O_2(g) \quad \Delta G = 717.5\ kJ\ mol^{-1},\ V^0 = 1.986\ V \tag{2}$$

Therefore, Ge nanowires can be first generated at the initial stage of the electrolytic reaction. As the reaction proceeds, a new layer of Si tends to appear around the surface of crystalline Ge due to their similar cubic crystal structures (Space group: *Fd3m*; lattice parameters: 5.6576 Å for Ge vs. 5.4309 Å for Si), leading to the formation of Ge@Si core–shell nanostructures (denoted as Ge@Si). Interestingly, the high-temperature environment of molten chlorides and the comparable crystallographic structures between crystalline Si and Ge can facilitate solid diffusion process in Ge@Si governed by the nanoscale Kirkendall effect to form SiGe alloy.[9,35–38] The driving force of solid diffusion in a binary alloy is generally explained as minimization of total Gibbs free energy and the presence of Ge at the surface of the SiGe alloy is energetically favorable because Ge has lower surface energy than Si.[20] Hence, the outward diffusion of Ge species is faster than the inward diffusion of Si species in the Ge@Si core–shell nanowires, thus generating internal voids. As a result, the transformation from the core–shell Ge@Si nanowires to SiGe alloy nanotubes is favorable.

The first demonstration of the above synthesis procedure is the preparation of SiGe alloy nanotubes. GeO_2 particles with a diameter of around 200 nm and SiO_2 spheres with diameters ranging from 2–10 μm are employed as starting reagents (Figure S1a,b, Supporting Information). Upon electrolysis of individual GeO_2 or SiO_2 particles at 2.1 V for 12 h, Ge or Si particles are generated according to the X-ray diffraction (XRD) results in Figure 2a. The lattice parameters for the electrolytically formed Ge or Si are calculated to be 5.65 or 5.43 Å, which agree well with the theoretical values. Energy-dispersive X-ray (EDX) spectra (Figure S2, Supporting Information) also confirm the purity of Ge or Si sample. Upon electrolysis of mixed oxides (Figure S1c, Supporting Information) under the same conditions, all the characteristic peaks of the electrolytic product can be well indexed to cubic crystalline SiGe alloy, suggesting the successful transformation of the mixture into crystalline SiGe alloy without noticeable signals of phase segregation. The (111) peak of the SiGe is located between those of the Si and Ge, revealing a lattice parameter of 5.60 Å (Figure 2b). The corresponding EDX spectrum indicates a Si/Ge atomic ratio of 1.12, which is close to the value in the reactants (Figure S2, Supporting Information).

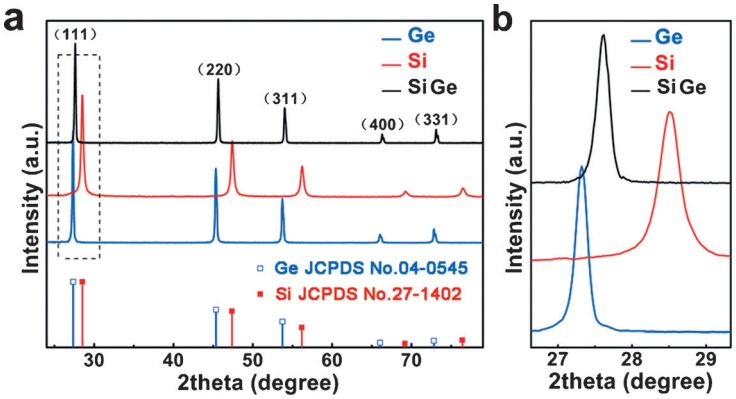

Figure 2. a) XRD patterns of Ge nanowires, Si nanowires, and SiGe nanotubes. b) The magnified region for the (111) peak shown in (a).

The morphology of these electrolytic products is characterized by field-emission scanning electron microscopy (FESEM) and transmission electron microscopy (TEM). Upon electrolysis of individual GeO_2 and SiO_2, solid nanowires are the predominant products in the electrolytic Si and Ge samples (Figure 3a,b). The as-obtained Ge nanowires have smaller diameters (80–100 nm) than that of Si nanowires (120–180 nm). These results confirm the successful synthesis of Si and Ge nanostructures through the template-free electro-reduction in molten chlorides. While as shown in Figure 3c, the electrolytic SiGe product exhibits a typical tubular-like nanostructure with open ends. The hollow interior of the alloy sample is further elucidated by the striking contrast between the center and the edge in the TEM observation (Figure 3d). Consistent with XRD analysis, the high-resolution TEM (HRTEM) image shows the crystalline nature of the SiGe nanotubes with a specific *d*-spacing of about 0.32 nm, corresponding to (111) planes of cubic SiGe crystals (Figure S3a). According to the N_2 sorption measurement (Figure S4), the Brunauer-Emmett-Teller (BET) specific surface area of the SiGe alloy nanotubes is about 26 $m^2 g^{-1}$, which is slightly higher than that of Si (24 $m^2 g^{-1}$) or Ge nanowires (14 $m^2 g^{-1}$). To further understand the structural evolution process, time dependent experiments have been conducted to gain better insight. Upon electrolysis for 5 h, core–shell Ge@Si nanowires are generated with a Ge-rich core and a Si-rich shell (Figure 3e). The electron scattering cross section of the Ge atom is larger than that of Si.[39]

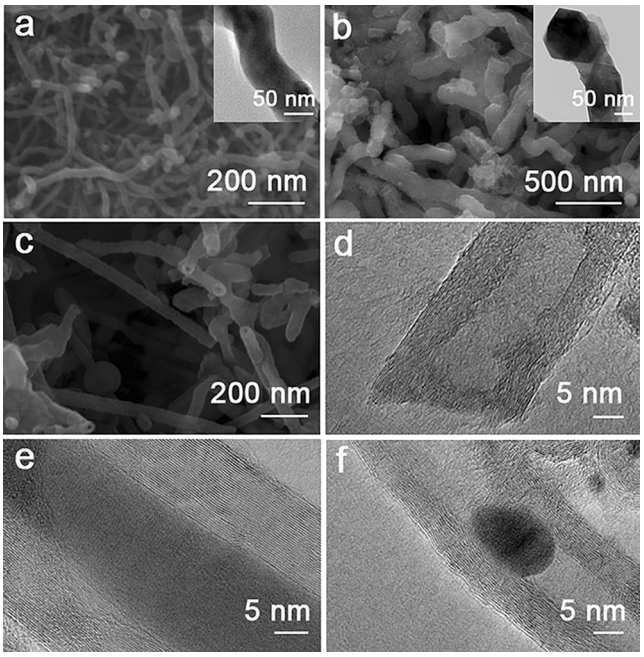

Figure 3. FESEM and TEM images of a) Ge nanowires, b) Si nanowires, and c),d) SiGe nanotubes obtained upon electrolysis at 2.1 V for 12 h and the intermediate products obtained upon electrolysis for e) 5 h and f) 8 h.

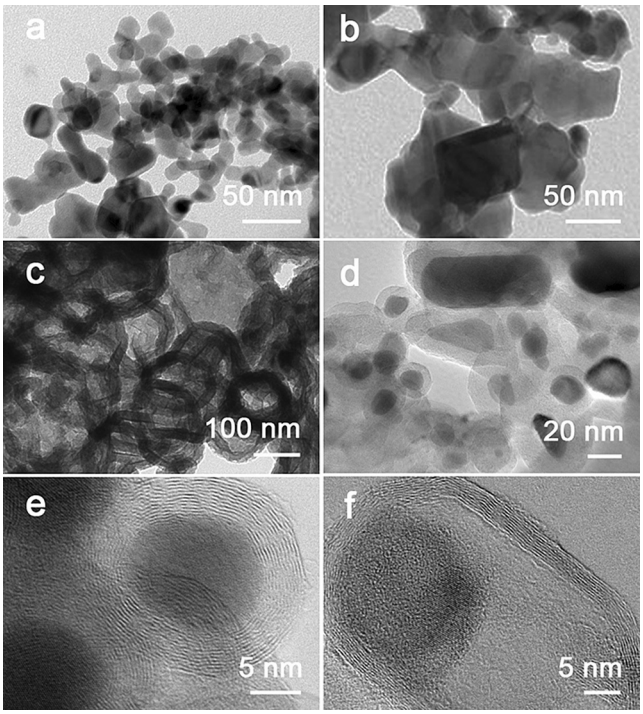

Figure 4. TEM images of a) Ge particles, b) Si particles, and c) SiGe hollow nanospheres obtained upon electrolysis at 2.3 V for 12 h and the intermediate products obtained upon electrolysis for d),e) 5 h and f) 8 h.

Consequently, the SiGe alloy domain appears lighter than the pure Ge core. A clear set of distinct lattice fringes with a spacing of 0.32 nm can be observed in the HRTEM image of the shell (Figure S3 b), indicating its crystalline nature. As mentioned before, the nanoscale Kirkendall effect in solid diffusion process within the SiGe alloy induces the formation of internal voids. Interestingly, such a morphological change can be clearly observed in the sample upon reaction for 8 h (Figure 3 f). To verify the formation of SiGe alloy, elemental mapping measurement has been performed on an individual Ge@Si core–shell nanowire (Figure S5 a) and an individual SiGe alloy nanotube (Figure S5 d) under TEM observation. The individual element mappings confirm the presence of the Ge core and Si shell within the nanowire (Figure S5 b,c) and the uniform distribution of Si and Ge elements in the final alloy nanotube (Figure S5 e,f). These results together with the XRD results confirm the formation of SiGe alloy nanotubes.

Importantly, the present electrolytic process described above is quite general and can be extended to prepare SiGe alloy hollow particles at higher overpotentials (Figure 4). Irregular Ge nanoparticles and Si nanoparticles are generated upon electrolysis of GeO_2 and SiO_2 respectively at 2.3 V for 12 h (Figure 4 a,b). Using mixed precursors of GeO_2 and SiO_2 particles, sphere-like hollow particles of SiGe alloy can be obtained upon the same electrolysis process (Figure 4 c and Figure S6). A similar structural evolution from the Ge@Si core–shell particles to the SiGe hollow particles is observed (Figure 4 d–f). It should be pointed out that Si and Ge could form a solid solution of any stoichiometry, which might enable the further regulation of SiGe hollow structures with adjustable composition (Figure S7).

The as-obtained SiGe alloy nanotubes, Si nanowires and Ge nanowires are evaluated as negative electrodes for LIBs. Figure 5 a gives the representative cyclic voltammetry (CV) curves of SiGe alloy nanotubes. In the first cathodic scan, a broad shoulder in the range from 1.2 to 0.6 V can be identified, which disappears in the following cycles. This broad peak can be associated with the irreversible formation of solid electrolyte interface (SEI). The other cathodic peak at around 0.35 V can be related to the reversible alloying reaction of Li_xM (M = Si, Ge). In the anodic scans, two overlapped peaks located at 0.45 and 0.55 V can be assigned to reversible delithiation of Li_xM alloy to amorphous Si and Ge nanoparticles. Another anodic peak at 1.2 V can be ascribed to the re-oxidation of surface Ge to GeO_2.[40] The slight decrease in the peak intensity in the subsequent scans indicates that some irreversible processes might have taken place during the first cycle.

Figure 5 b displays the charge–discharge voltage profiles of the prepared SiGe nanotubes. The first discharge (lithium insertion) and charge capacities are 2362 and 1146 mAh g^{-1} respectively, resulting in a low Coulombic efficiency of 48.5 % in the first cycle. The initial irreversible capacity loss is mainly caused by the decomposition of electrolyte and the formation of SEI film, which is a common drawback for nanostructured anodes. The Coulombic efficiency increases to 96 % after the first 5 cycles, indicating good stability of the nanotube electrode. The cycling performance for the prepared SiGe nanotubes is shown in Figure 5 c at a constant current density of 200 mA g^{-1} between 0.01 and 1.5 V. After 100 cycles, the prepared SiGe nanotube electrode still delivers a high

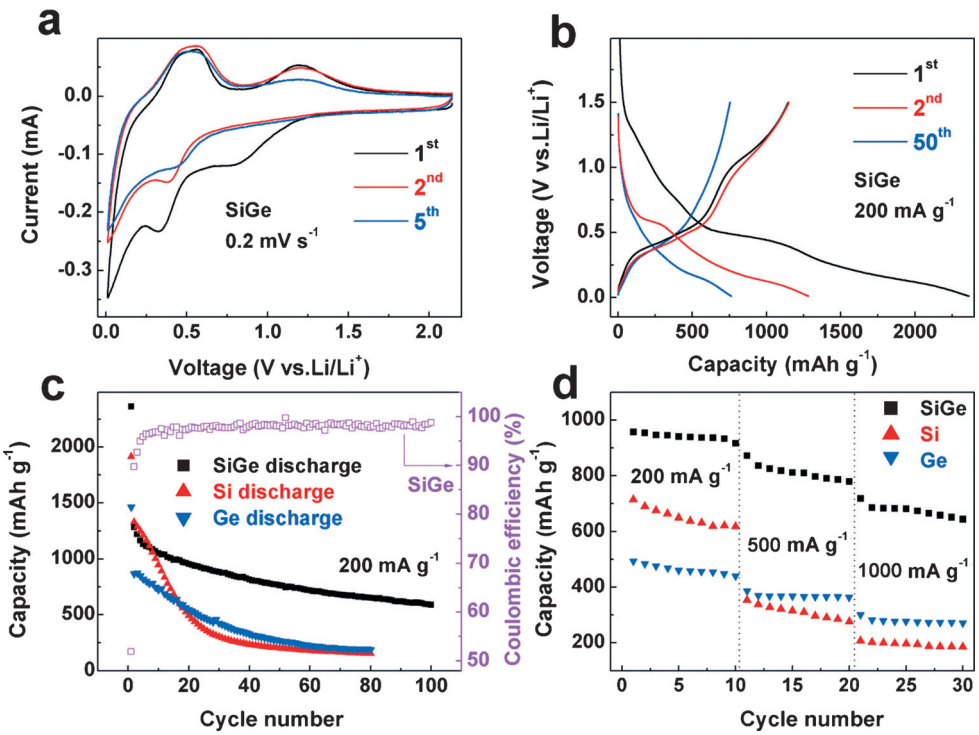

Figure 5. a) CV curves at 0.2 mV s^{-1} and b) galvanostatic charge–discharge voltage profiles of the SiGe nanotube electrode at 200 mA g^{-1}. c) Cycling performance of the SiGe nanotubes, Si nanowires, and Ge nanowires and the corresponding Coulombic efficiency of SiGe product at 200 mA g^{-1}. d) Rate capabilities of the SiGe nanotubes, Si nanowires and Ge nanowires after cyclic voltammetry scans for 5 cycles at 0.2 mV s^{-1}.

reversible capacity of 590 mAh g^{-1}. The corresponding Coulombic efficiency increases rapidly over the course of the first few cycles and remains at almost 100% afterwards. The cycling performance for the Si nanowire and Ge nanowire electrodes are also presented for comparison. Compared to the SiGe nanotube electrode, the specific capacity for the Si nanowire electrode experiences a rapid drop within the first 20 cycles. As for the Ge nanowire electrode, the specific capacity is much lower than that of the SiGe and Si electrodes, and it also exhibits a rapid decay. Compared with these solid nanowires, the SiGe nanotubes exhibit much better cyclic capacity retention from the second cycle onward. The enhanced cycling stability of SiGe nanotubes can be attributed to the unique hollow structure that can effectively accommodate structural strain upon repeated insertion and extraction of Li^+ ions. The rate capability of the SiGe nanotube electrode after CV scans is also investigated as shown in Figure 5d (Figure S8, Supporting Information). The reversible lithium storage capacities of 916, 779, and 666 mAh g^{-1} can still be delivered in the SiGe nanotube electrode at 200, 500, and 1000 mA g^{-1}, respectively. The Ge and Si nanowires exhibit much inferior lithium storage performance compared with the SiGe nanotubes, indicating the structural and composition advantages of the alloy nanotubes.

In summary, we report an electro-reduction method in molten chlorides for synthesis of crystalline SiGe hollow nanostructures with controllable morphologies. By simply tailoring electrolysis voltages, SiGe alloy nanotubes and hollow particles could be controllably prepared. Importantly, solid diffusion process in Ge@Si core–shell structures governed by the nanoscale Kirkendall effect leads to the generation of internal voids for the hollow structures. The unique structural and composition merits endow the SiGe nanotubes with enhanced lithium-storage performance compared with the individual solid components.

Acknowledgements

X.W. and D.H.W. acknowledge the funding support by the National Natural Science Foundation of China (51325102), the Natural Science Foundation of Ningxia (NZ14001), and the Young-talent Chenguang Project of Wuhan City. X.W.L. acknowledges the funding support by the Ministry of Education of Singapore through Academic Research Fund (AcRF) Tier 1 (M4011154; RG12/13).

Keywords: alloys · germanium · lithium-ion batteries · nanotubes · silicon

How to cite: *Angew. Chem. Int. Ed.* **2016**, *55*, 7427–7431
Angew. Chem. **2016**, *128*, 7553–7557

[1] X. Y. Yu, L. Yu, X. W. Lou, *Adv. Energy Mater.* **2015**, *6*, 1501333.
[2] J. Liu, J. G. Zhang, Z. G. Yang, J. P. Lemmon, C. Imhoff, G. L. Graff, L. Y. Li, J. Z. Hu, C. M. Wang, J. Xiao, G. Xia, V. V. Viswanathan, S. Baskaran, V. Sprenkle, X. L. Li, Y. Y. Shao, B. Schwenzer, *Adv. Funct. Mater.* **2013**, *23*, 929.
[3] D. Larcher, J. M. Tarascon, *Nat. Chem.* **2015**, *7*, 19.
[4] N. Liu, L. Hu, M. T. McDowell, A. Jackson, Y. Cui, *ACS Nano* **2011**, *5*, 6487.
[5] Y. Yao, M. T. McDowell, I. Ryu, H. Wu, N. A. Liu, L. B. Hu, W. D. Nix, Y. Cui, *Nano Lett.* **2011**, *11*, 2949.
[6] M. H. Park, K. Kim, J. Kim, J. Cho, *Adv. Mater.* **2010**, *22*, 415.
[7] J.-K. Yoo, J. Kim, Y. S. Jung, K. Kang, *Adv. Mater.* **2012**, *24*, 5452.
[8] N. Lin, Y. Han, L. Wang, J. Zhou, J. Zhou, Y. Zhu, Y. Qian, *Angew. Chem. Int. Ed.* **2015**, *54*, 3822; *Angew. Chem.* **2015**, *127*, 3893.
[9] M.-H. Park, Y. Cho, K. Kim, J. Kim, M. Liu, J. Cho, *Angew. Chem. Int. Ed.* **2011**, *50*, 9647; *Angew. Chem.* **2011**, *123*, 9821.
[10] K. H. Seng, M.-H. Park, Z. P. Guo, H. K. Liu, J. Cho, *Angew. Chem. Int. Ed.* **2012**, *51*, 5657; *Angew. Chem.* **2012**, *124*, 5755.
[11] X. L. Wu, Y. G. Guo, L. J. Wan, *Chem. Asian J.* **2013**, *8*, 1948.
[12] L. Li, K. H. Seng, C. Feng, H. K. Liu, Z. Guo, *J. Mater. Chem. A* **2013**, *1*, 7666.

[13] N. Lin, L. B. Wang, J. B. Zhou, J. Zhou, Y. Han, Y. C. Zhu, Y. T. Qian, C. H. Cao, *J. Mater. Chem. A* **2015**, *3*, 11199.
[14] Y. J. Yu, C. Yue, S. B. Sun, W. Lin, H. Su, B. B. Xu, J. T. Li, S. T. Wu, J. Li, J. Y. Kang, *ACS Appl. Mater. Interfaces* **2014**, *6*, 5884.
[15] T. Kennedy, M. Bezuidenhout, K. Palaniappan, K. Stokes, M. Brandon, K. M. Ryan, *ACS Nano* **2015**, *9*, 7456.
[16] T. Song, H. Cheng, H. Choi, J.-H. Lee, H. Han, D. H. Lee, D. S. Yoo, M.-S. Kwon, J.-M. Choi, S. G. Doo, H. Chang, J. Xiao, Y. Huang, W. I. Park, Y.-C. Chung, H. Kim, J. A. Rogers, U. Paik, *ACS Nano* **2012**, *6*, 303.
[17] T. Song, H. Y. Cheng, K. Town, H. Park, R. W. Black, S. Lee, W. I. Park, Y. G. Huang, J. A. Rogers, L. F. Nazar, U. Paik, *Adv. Funct. Mater.* **2014**, *24*, 1458.
[18] M. Ben-Ishai, F. Patolsky, *Adv. Mater.* **2010**, *22*, 902.
[19] D. Duveau, B. Fraisse, F. Cunin, L. Monconduit, *Chem. Mater.* **2015**, *27*, 3226.
[20] H. Kim, Y. Son, C. Park, M. J. Lee, M. Hong, J. Kim, M. Lee, J. Cho, H. C. Choi, *Nano Lett.* **2015**, *15*, 4135.
[21] C. Liu, F. Li, L. P. Ma, H. M. Cheng, *Adv. Mater.* **2010**, *22*, E28.
[22] Y. S. Li, J. L. Shi, *Adv. Mater.* **2014**, *26*, 3176.
[23] Z. Y. Wang, L. Zhou, X. W. Lou, *Adv. Mater.* **2012**, *24*, 1903.
[24] X. Y. Lai, J. E. Halpert, D. Wang, *Energy Environ. Sci.* **2012**, *5*, 5604.
[25] W. Wei, Z. H. Wang, Z. Liu, Y. Liu, L. He, D. Z. Chen, A. Umar, L. Guo, J. H. Li, *J. Power Sources* **2013**, *238*, 376.
[26] T. Song, J. L. Xia, J. H. Lee, D. H. Lee, M. S. Kwon, J. M. Choi, J. Wu, S. K. Doo, H. Chang, W. Il Park, D. S. Zang, H. Kim, Y. G. Huang, K. C. Hwang, J. A. Rogers, U. Paik, *Nano Lett.* **2010**, *10*, 1710.
[27] M. Ben-Ishai, F. Patolsky, *J. Am. Chem. Soc.* **2009**, *131*, 3679.
[28] W. Xiao, X. Jin, G. Z. Chen, *J. Mater. Chem. A* **2013**, *1*, 10243.
[29] W. Xiao, D. Wang, *Chem. Soc. Rev.* **2014**, *43*, 3215.
[30] J. Y. Yang, S. G. Lu, S. R. Kan, X. J. Zhang, J. Du, *Chem. Commun.* **2009**, 3273.
[31] H. Yin, W. Xiao, X. Mao, W. Wei, H. Zhu, D. Wang, *Electrochim. Acta* **2013**, *102*, 369.
[32] H. Yin, W. Xiao, X. Mao, H. Zhu, D. Wang, *J. Mater. Chem. A* **2015**, *3*, 1427.
[33] J. Zhao, J. Li, P. Ying, W. Zhang, L. Meng, C. Li, *Chem. Commun.* **2013**, *49*, 4477.
[34] S. K. Cho, F. R. F. Fan, A. J. Bard, *Angew. Chem. Int. Ed.* **2012**, *51*, 12740; *Angew. Chem.* **2012**, *124*, 12912.
[35] Y. Son, Y. Son, M. Choi, M. Ko, S. Chae, N. Park, J. Cho, *Nano Lett.* **2015**, *15*, 6914.
[36] H. J. Fan, U. Goesele, M. Zacharias, *Small* **2007**, *3*, 1660.
[37] Y. D. Yin, R. M. Rioux, C. K. Erdonmez, S. Hughes, G. A. Somorjai, A. P. Alivisatos, *Science* **2004**, *304*, 711.
[38] J. Liang, X. Li, Q. Cheng, Z. Hou, L. Fan, Y. Zhu, Y. Qian, *Nanoscale* **2015**, *7*, 3440.
[39] Y. Y. Wu, R. Fan, P. D. Yang, *Nano Lett.* **2002**, *2*, 83.
[40] K. H. Seng, M.-H. Park, Z. P. Guo, H. K. Liu, J. Cho, *Nano Lett.* **2013**, *13*, 1230.

Received: March 16, 2016
Published online: May 9, 2016

